Negative refraction, subwavelength focusing and beam formation by photonic crystals

Ekmel Ozbay, Koray Aydin, Irfan Bulu and Kaan Guven

Nanotechnology Research Center, Department of Physics, Department of Electrical and Electronics Engineering, Bilkent University, Bilkent, 06800 Ankara, Turkey

E-mail: ozbay@bilkent.edu.tr

Abstract
We present a review of our experimental and numerical studies on the negative refraction related phenomena in two-dimensional dielectric photonic crystals (PCs). By employing photonic bands with appropriate dispersion, the propagation of the electromagnetic wave through a PC can be controlled to a large extent, and diverse and completely novel electromagnetic phenomena can be generated. We perform the spectral analysis of the negative refraction arising from a convex TM polarized photonic band of a hexagonal PC. As a consequence of negative refraction, we demonstrate a photonic crystal flat lens, which has the ability to focus electromagnetic waves and provide subwavelength resolution laterally. Finally, a photonic crystal with an embedded source is shown to provide a highly directional beam, which can be utilized in certain antenna applications.

(Some figures in this article are in colour only in the electronic version)

1. Introduction

Photonic crystals (PCs) are periodically modulated dielectric or metallic structures, which are envisaged as the building block of the next generation of integrated optical devices [1,2]. The periodicity gives rise to bands for the propagation of electromagnetic waves and band gaps, where the propagation is prohibited for a certain frequency range, in close analogy of the photon to an electron moving in a periodic electric potential in a solid. By employing different dielectric materials and different geometries in the fabrication of the PC, the band structure and hence the propagation of light can be modified virtually in any way in a controllable manner. In particular, two-dimensional (2D) PC structures stand out for their potential use in planar integrated photonic circuits. They also provide a convenient framework to investigate novel electromagnetic phenomena, since 2D PCs are easier to fabricate compared with their 3D counterparts. An essential feature is the scalability of the governing Maxwell's equations; this enables the straightforward projection of an existing PC design to different scales ranging from microwave up to far-infrared.

On the other hand, most of the target applications reside in the near-infrared (communication) and optical wavelengths which require submicron scale PCs. At present, the realization of PC-based devices at this scale is still experimental [3–9]. When contrasted to the required level of uniformity of the PCs, the existing fabrication technologies still need further advancement. In this paper, we shall restrict our discussion to the electromagnetic properties of microwave PCs and leave the fabrication issues aside.

Most of the studies on PCs first addressed the utilization of the photonic band-gaps [10], localized photon states [11], band-edges [12], defect modes [13, 14] and coupled cavity waveguides [15–20]. On the other hand, the investigation of the dispersion of photonic bands revealed diverse and novel electromagnetic phenomena. In particular, it was demonstrated that the PCs refract the electromagnetic waves in an unusual manner, including negative refraction, although the PC is a positive medium intrinsically [21–29].

In this paper, we review our studies involving the negative refraction phenomenon in 2D dielectric PCs. The paper is organized as follows: in the next section, the spectral
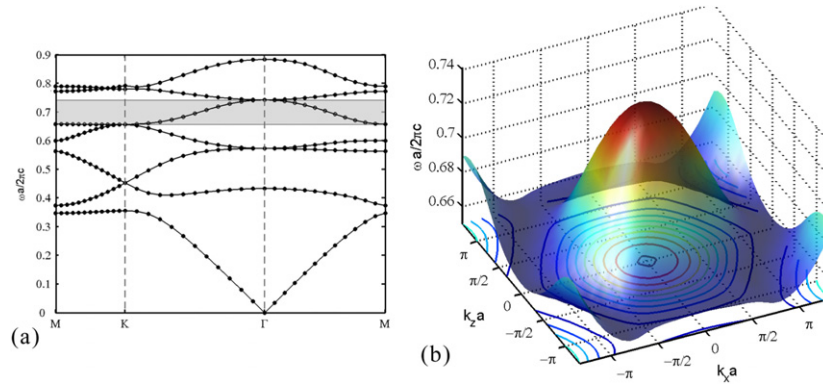
Figure 1. (*a*) TM polarized band structure of the hexagonal PC. The 5th band (shaded) is used to generate negative refraction. (*b*) The frequency surface of the 5th band in the full Brillouin zone. Some EFCs are projected to the Brillouin zone plane.

investigation of the negative refraction originating from a transverse-magnetic (TM) polarized PC band is presented by experiment and simulation. In this context, the mechanism arising from the band structure which generates the negative refraction is discussed. We then consider the focusing of EM waves emitted by omnidirectional sources to demonstrate that the PC-based lenses can achieve subwavelength resolution surpassing their conventional (positive refractive index) counterparts. The flat lens behaviour (i.e. absence of an optical axis) for PC slab lens is obtained.

A target application area involving PCs is antennas in communication systems. For this purpose, we demonstrate the shaping of the radiation pattern of an omnidirectional antenna embedded into a PC. The radiation of the antenna couples to a particular photonic band propagating through the PC and then gets emitted through the PC surface with high directivity. This type of beam formation is important for certain applications.

2. Spectral analysis of the negative refraction by a 2D photonic crystal slab

We have designed and constructed a PC consisting of a square array of cylindrical alumina rods with dielectric constant $\varepsilon = 9.61$, diameter 3.15 mm and length 150 mm. The lattice constant is $a = 4.79$ mm. The TM polarized (i.e. electric field vector, $\boldsymbol{E}$, is parallel to the rods) band structure of the PC is calculated by plane wave expansion method (figure 1(*a*)). We focus on the 5th band shaded in the figure, which extends from $\tilde{\omega} = 0.65$ ($f = 40.65$ GHz) to $\tilde{\omega} = 0.74$ ($f = 46.27$ GHz), where $\tilde{\omega} = \omega a/2\pi c$ is the scaled frequency. In figure 1(*b*), the band surface in the full Brillouin zone is shown and several equal frequency contours (EFCs) projected to the plane are indicated. The EFCs of the band shrink with increasing frequency, contrary to the EFCs in air ($n = 1$) which are given by the dispersion $\omega = ck$. As a result, the effective refractive index $n_{\text{eff}} = \text{sgn}(\vec{v}_g \cdot \vec{k}_f)(c|\vec{k}_f|/\omega)$ becomes negative due to the sign of the antiparallel group velocity $\vec{v}_g = \nabla_{\vec{k}}\omega$ and the phase velocity $\vec{v}_p = (c/|n_{\text{eff}}|)\hat{k}_f$ [25–27]. Here c is the speed of light in vacuum and $\hat{k}_f$ is the unit wavevector in the PC.

The experiment setup to measure the negative refraction consists of a network analyzer and a set of transmitter-receiver antennas. The PC has 7 layers along the incidence (ΓM) direction and 31 layers along the lateral (ΓK) direction. The
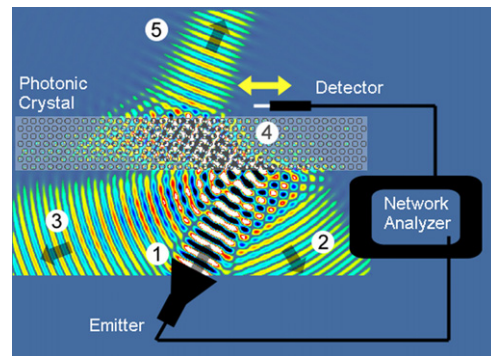

Figure 2. The intensity map obtained by simulation. The microwave signal is incident to the PC at an angle of 30°. Reflected and refracted components are marked (see text for description). The measurement setup is superposed on the image to provide visual description of the experiment. The double arrow indicates the lateral scanning directions.

field is incident from the negative side of the PC with respect to its central axis. Along the other side of the PC, the spatial distribution of the transmitted signal is scanned in 1.27 mm steps. The frequency is swept from 38.5 to 43.5 GHz covering the lower half of the 5th band (frequencies above 44 GHz were beyond the measuring capability of the present equipment). Figure 2 shows the experimental setup along with an FDTD simulation for $\theta_i = 30°$ incidence (mark 1) at frequency $\tilde{\omega} = 0.667$ ($f = 41.7$ GHz). At this frequency, reflection (mark 2) and diffraction (mark 3) occur since the condition $\tilde{\omega} \leqslant a/(2a_{\text{interface}})$ is not met (24, 26). Here, $a_{\text{interface}}$ is the period along the interface (surface) of the PC. For the hexagonal PC, $a_{\text{interface}} = a$ for the interface normal to the ΓM direction; hence, the above condition reads $\tilde{\omega} \leqslant 0.5$. Violating this condition may generate higher order Bragg reflections for higher angles of incidence, as exemplified here. Nevertheless, the transmitted beam (marks 4 and 5) appears to be a single component. Hence, we will employ Snell's law to extract the n_{eff} from the measurements.

In figure 3, the transmission spectra are shown as a function of frequency and lateral position for three different incidence angles of $\theta_i = 15°$, 30° and 45°. Evidently, the transmitted beam appears on the negative side in agreement with the simulation [29]. In figure 3(*b*), the intensity profiles at $f = 41.7$ GHz are plotted. The incident field has a Gaussian
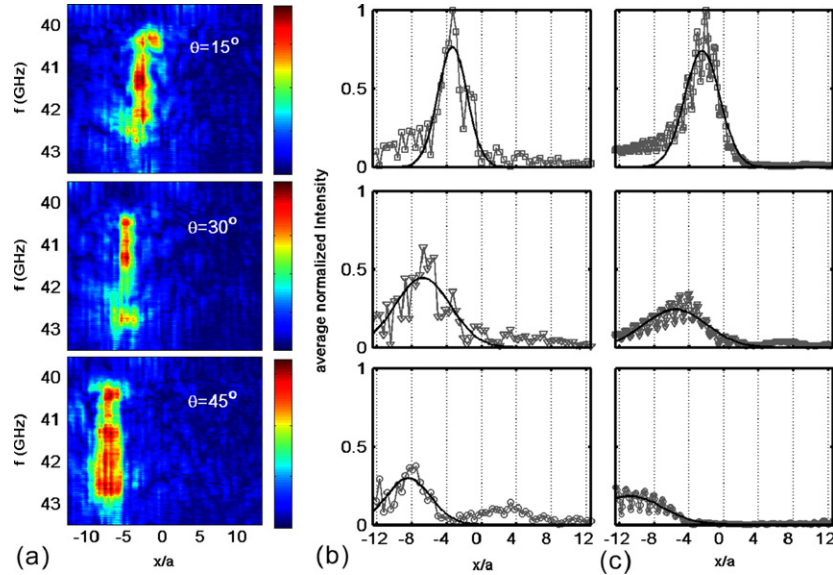
Figure 3. (*a*) The measured negative refraction spectra of the 5th band along the PC-air interface for incidence angles $\theta = 15°$, $30°$ and $45°$. Measured (*b*) and simulated (*c*) intensity profiles at $f = 41.7$ GHz for the respective incidence angles. Solid curves are Gaussian fits.

beam profile centred at $x = 0$ (not shown in the figure). The intensities are normalized with respect to the maximum intensity for the 15° incidence. The profiles shift in accordance with increasing incidence angle. The shift is accompanied by a decrease in the transmission intensity which is mainly due to the increased reflection for oblique incidence. The intensity profiles obtained from FDTD simulations in figure 3(*c*) show good agreement with the experimentally measured profiles.

Using Snell's law for this geometry $n(\omega) \sin \theta_f = n_{\text{air}} \sin \theta_i$, where θ_i is the angle of incidence and θ_f is the angle of refraction inside the PC, we obtain from the experiment $n_{\text{eff}} = -0.52$, -0.66 and -0.86 for $\theta_i = 15°$, $30°$ and $45°$, respectively. The simulation results for the same incidence angles give $n_{\text{eff}} = -0.66$, -0.72 and -0.80, respectively. It is evident that $n_{\text{eff}}(\omega)$ bears the anisotropy of the band structure, particularly at the lower band edge where the EFCs start to deviate significantly from the circular shape. This necessitates the fine tuning of the material parameters to achieve circular EFCs in the band structure, so that the angular anisotropy is eliminated. We would like to stress that the $n_{\text{eff}}(\omega)$ introduced for PCs does not intend to describe the optical properties in terms of a homogeneous medium. Furthermore, one should note that the propagation of electromagnetic waves within the PC occur via Bloch modes, and not similar to a homogeneous medium.

3. Subwavelength focusing by using a 2D photonic crystal slab lens

In this study we construct a cubic PC with the same alumina rods described in the previous section. The lattice constant is $a = 4.79$ mm. We employ the first band of the PC for generating negative refraction. In this case, the part of the band with convex EFC is centred around the M point (figure 4). As indicated in [24], the EFCs are required to be both convex and larger than the EFCs in freespace, in order to obtain negative refraction. However, in this case $k \cdot \partial\omega/\partial k \geqslant 0$ everywhere
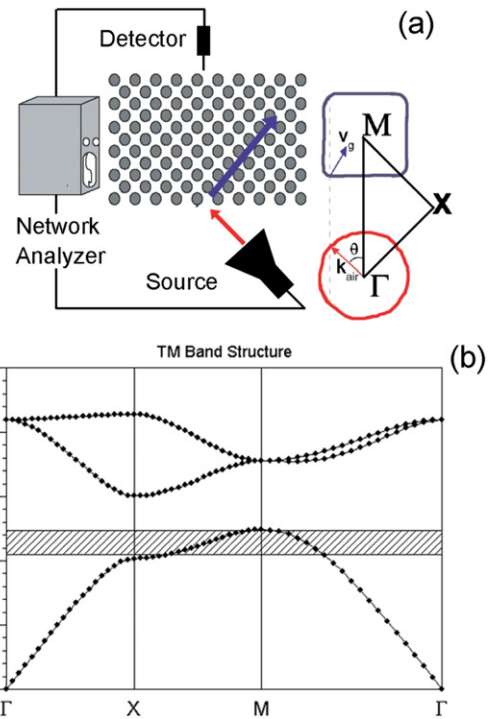

Figure 4. (*a*) (Left) The schematic view of the experiment setup. The square PC slab is depicted by the array of grey dots. (Right) The respective EFCs of the electromagnetic wave at $\tilde{\omega} = 0.2189$ are depicted in freespace and in the PC. The conservation of surface-parallel wave vector gives the direction of the refracted waves inside the PC. (*b*) The band structure of the cubic PC. The shaded region between $\tilde{\omega} = 0.2093$ and $\tilde{\omega} = 0.2467$ gives negative refraction.

within the first Brillouin zone, and the group- and phase-velocities are not antiparallel [22, 24–27]. For comparison, the relevant band of the PC discussed in the previous section was centred around the Γ point, and the behaviour of the PC medium was resembling a true left-handed (i.e. negative index)

medium. This time we have a right-handed (positive index) PC which is just exhibiting negative refraction. The advantage of using the first band is that, since $\lambda > 2\sqrt{2}a$, the propagation does not suffer from Bragg reflections inside the PC and a well-defined single beam propagation is guaranteed within the PC. The scaled frequency range that gives negative refraction extends from $\tilde{\omega} == 0.2093$ to $\tilde{\omega} = 0.2467$.

By using the setup depicted in figure 4(a), the negative refraction in this PC has been verified by scanning the lateral profiles of the incident and transmitted signals [29]. Based on the presence of negative refraction, we would like to investigate the focusing phenomenon in this PC.

Superlensing, which is not limited by diffraction, was proposed first by Pendry, as a negative refraction-induced phenomenon [31]. Ideally, this requires an isotropic index of refraction of negative unity and amplification of evanescent field modes while propagating across the lens structure which then contribute for an immaculate image formation on the focal plane. Anisotropy and deviations from negative unity will result in an impaired focusing, but still exhibit unusual focusing properties in contrast to positive refractive index materials. Following the prediction by Pendry on the perfect focusing by negative refraction [31] and initial theoretical studies concerning PCs [24], the subwavelength focusing by PCs were demonstrated experimentally [28, 29]. This quickly led to an extensive literature on the subject [24–38].

In this study, we use a PC slab having 17 layers in the propagation direction and 21 layers in the lateral direction. The operation frequency is set to $f = 13.698$ GHz. At this frequency, the overlap of the respective EFCs in freespace and in PC provides the largest angular range for negative refraction and thus better isotropy in focusing [24, 29]. Two point sources which are separated by a distance of $\sim\lambda/3$ (i.e. within subwavelength separation) are placed 0.7 mm away from the air–PC interface and the lateral profile of the transmitted signal is scanned at 0.7 mm away from the PC–air interface. We also simulated this experimental configuration using the FDTD method. Figure 5(a) shows that the sources can be resolved individually in the transmitted signal profile. The full width at half maximum (FWHM) of the individual source peaks is approximately 0.21λ. For comparison, the calculated FWHM of the transmitted signal from a single source in the absence of the PC was found to be 5.94λ. We also note the good agreement between the simulated and measured data. When the crystal is removed, no features are visible on the intensity profile (dashed line).

When the two sources are fed by the same signal generator, they radiate coherently. It is then possible to see interference peaks in the resulting radiation pattern which may be incorrectly attributed to a subwavelength focusing ability by the PC. To avoid such interference effects, we repeated the experiment using two separate (incoherent) point sources having frequencies 13.698 GHz and 13.608 GHz, respectively. Independent signal generators are used for driving the monopole antennas to ensure incoherent behaviour, and a powermeter is used for the measurement. Again, the individual peaks corresponding to each source are clearly resolved (figure 5(b)).

The incoherent source setup was simulated for a uniform dielectric slab with a high refractive index to check whether
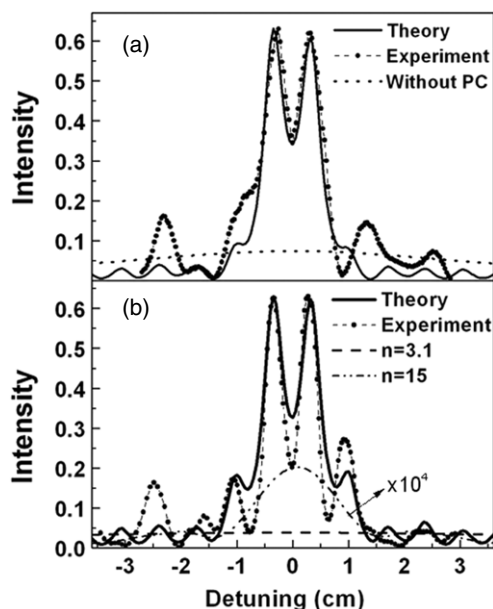

Figure 5. Subwavelength resolution: (a) measured ($\cdots$) and simulated (——) power distribution at 0.7 mm away from the PC–air interface for two coherent sources separated by $\lambda/3$ at 0.7 mm away from the air–PC interface. The dotted line denotes the simulated intensity profile in the absence of PC. (b) Same setup with two incoherent point sources. The lower dashed and dashed–dotted curves indicate the power distribution for uniform dielectric slabs with refractive indices $n = 3.1$ and $n = 15$, respectively. Note the magnification of the curve.

the observed resolution originates from the refractive index contrast as in the case of oil (or solid) immersion microscopy. The dashed and dashed–dotted lines in the bottom panel of figure 5 indicate the power distribution in the presence of a dielectric slab of $n = 3.1$ and $n = 15$, respectively. Note that $n = 3.1$ is also the refractive index of the alumina rods used in constructing the photonic crystal. Even with the use of unrealistically high refractive index ($n = 15$), the sources are not resolved. Besides, the large reflection due to high index contrast at the interface significantly reduces the transmitted power when compared with the high (63%) transmission obtained from the photonic crystal at this operating frequency. So, even if the observed subwavelength is associated with near field effects, this is not achievable by ubiquitous materials.

As the theoretical studies indicated [32], the subwavelength resolution is due to the amplification of evanescent wavevectors by the medium and their transfer between the interfaces of the medium. In the case of PCs, the periodicity imposes an upper cut-off to the transverse wave vector that can be amplified, which brings an ultimate limit to the superlens resolution. Materials with true intrinsic negative index of refraction do not have such limitation. Evidently, the source and image plane should be close to the PC interfaces so that the evanescent modes of the source can be picked up by the PC and then be detected at the other interface.

4. Highly directional radiation from a plain photonic crystal with an embedded source

The ability to control the propagation of electromagnetic waves by PCs brings naturally the possibility of generating
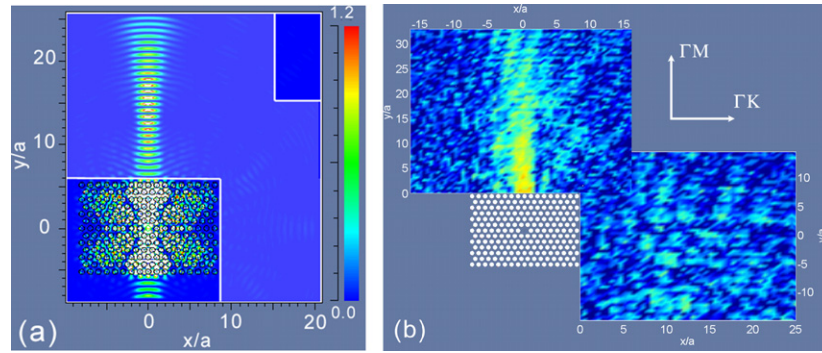
Figure 6. (*a*) The simulated and (*b*) experimentally measured TM field intensity pattern of a source with $f = 41.9$ GHz located at the centre of the PC over a rectangular area. The hexagonal PC is a 17×13 layer rectangular slab. The light shaded area in the simulation map corresponds roughly to the regions scanned experimentally.

highly directional radiation from omnidirectional sources. Some studies utilize the PC as a cover or substrate to an externally located source [39–41]. Other studies consider embedded sources in PCs where the directivity was achieved by employing localized cavity modes [42], generating partial gaps in the band structure by stretching of the crystal structure spatially [43], photonic band edges [44, 45], corrugated surface modes [46, 49], and self guiding modes governed by flat photonic bands [47, 48].

In this section, we present yet another example in which the directional beam is generated by a plain bulk photonic crystal without any modification to its geometrical and material parameters. Employing a photonic band with appropriate topology suffices to channel the radiation of the embedded source and then transfer it to the free-space in the form of a directional beam. The lateral isolation of the emitted radiation within the PC is achieved by a compact size.

We use the 5th photonic band of the PC described in detail in section section 2. We note that the equal frequency contours (EFCs) depicted in figure 1(*b*) are of hexagonal shape at the lower part of the band with nearly flat edges normal to the ΓM direction. It has been shown that the Bloch modes within the PC possess even symmetry when the wavevector, $\boldsymbol{k}$, is along the ΓM direction and odd symmetry when $\boldsymbol{k}$ is along the ΓK direction, whereas a plane wave propagating in freespace at normal incidence is of even symmetry [44]. When the surface geometry of the PC conforms to the band contours, the Bloch modes with matching symmetry can couple to the freespace with very high transmission. The flat band topology and the enhancement (or suppression) of transmission induced by the symmetry of the propagating modes provide the mechanism for the spatial guiding of the electromagnetic wave within the PC. At the interface, the electromagnetic wave will be refracted, which is again governed by the dispersion of the PC band. The mathematical formulation of the effective index of refraction for a PC band was given as $n_{\text{eff}} = \text{sgn}(\vec{v}_g \cdot \vec{k}_f)(c|\vec{k}_f|/\omega)$, where $\vec{v}_g = \vec{\nabla}_k \omega$ is the group velocity and $\vec{k}_f$ is the wavevector inside the PC. Based on this formulation, the flat segments of the band would lead to n_{eff} small in magnitude (since $\vec{\nabla}_k \omega$ becomes small) and the convexity brings the negative sign. For illustrative purpose, let us assume that the PC is a medium with $n_{\text{eff}} \approx 0$. Then, Snell's law at the PC–air interface $n_{\text{eff}} \sin \theta_i = \sin \theta_f$ implies that all incident waves would refract

almost parallel to the normal and hence would result in a highly directional beam.

The 2D PC has 17 layers along the x (ΓK) direction and 13 layers along the y (ΓM) direction. Figure 6(*a*) shows the 2D intensity pattern of the radiation at $f = 41.9$ GHz computed by FDTD simulation. The strong directivity of the radiation along the ΓM direction and the absence of any significant amount of radiation in the ΓK direction are clearly observed in this simulation. In figure 6(*b*), the experimental intensity pattern is plotted. The measurement is performed by a 2D spatial scanning setup and two monopole antennas, one inserted into the PC, the other mounted on the scanning probe. The transmission spectrum is measured by a network analyzer. The calibration measurement is taken in the absence of the PC, the scanning probe being located at $x = 0$ and at the y coordinate which corresponds to the location of the PC surface. The intensity map in figure 6(*b*) is combined from two separate measurements, each performed on a rectangular area in the ΓM and ΓK directions, respectively. The axes are scaled by the PC period. The colour mapped intensity scale of the experimental plot ranges from -20 to 10 dB. The directional beam emerging from the ΓM surface is clearly observable. Some background noise is present in comparison with the simulation, which is due to the reflections in the experiment environment, and the finite size of the PC normal to the measurement plane. In the simulations the PC extends infinitely along the out-of-plane direction.

The intensity map of the monopole antenna obtained in the (*a*) presence and (*b*) absence (i.e. freespace) of the photonic crystal are compared in figure 7. The respective lateral profiles of the beam at locations $y/\lambda = 0$, 5, 10 and 15 (relative to the PC surface) are plotted in figures 3(*c*) and (*d*). The intensity is normalized by the maximum intensity of the profile at the $y/\lambda = 0$ (PC surface location). The FWHM of the profiles obtained in the presence of the PC are 2.3λ, 2.0λ, 2.7λ and 3.3λ, respectively.

5. Conclusion

In this paper, we review our recent studies concerning the negative refraction and the focusing properties of 2D dielectric PCs. The mechanism leading to negative refraction originates from the convex topology of the particular photonic band structure, which can then be characterized by a negative effective index of refraction, n_{eff}. The spectral analysis of the
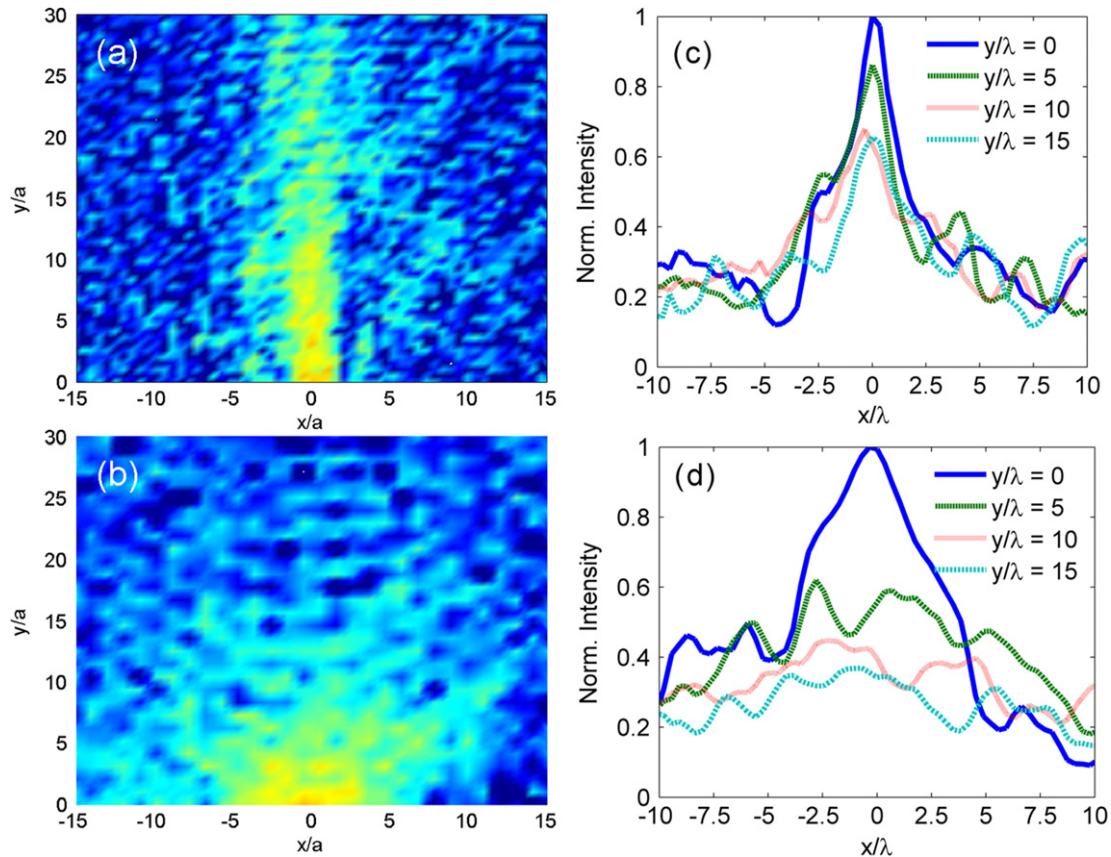
Figure 7. The experimental 2D intensity map along the ΓM direction starting from the PC surface location (*a*) when the monopole is embedded in the PC and (*b*) when the PC is removed (freespace propagation). (*c*) The lateral beam profile at locations $y/\lambda = 0$, 5, 10 and 15 taken from the map in (*a*). Intensity axis is normalized by the maximum of the respective $y/\lambda = 0$ profile.

negative refraction indicates that n_{eff} is in general anisotropic, particularly towards the band edges. The negative refraction enables the focusing of electromagnetic waves; hence, a PC slab can be utilized like a focusing lens. We demonstrate the focusing of the electromagnetic waves emitted by two point sources which are located close to the PC interface and separated from each within a subwavelength distance. The two sources can be clearly resolved by the PC lens. Finally, we employ a PC slab with an embedded point source to generate directional radiation. In this case, the flat dispersion of the photonic bands enables the guiding and spatial confinement of the radiation.

Acknowledgments

References

[1] Joannopoulos J D, Meade R D and Winn J N 1995 *Photonic Crystals: Molding the Flow of Light*, (Princeton, NJ: Princeton University Press)

[2] Soukoulis C M (ed) 2000 *Photonic Crystals and Light Localization in the 21st Century* (Dortrecht: Kluwer)

[3] Benisty H, Weisbuch C, Labilloy D, Rattier M, Smith C J M, Krauss T F, De La Rue R M, Houdré, Oesterle U, Jouanin C and Cassagne D 1999 *J. Lightwave Technol.* **17** 2063

[4] Krauss T, Song Y P, Thomson S, Wilkinson C D W and De La Rue R M 1994 *Electron. Lett.* **30** 1444

[5] Gourley P L, Wendt J R, Vawter G A, Brennan T M and Hammons B E 1994 *Appl. Phys. Lett.* **64** 687

[6] Noda S, Tomoda K, Yamamoto N and Chutinan A 2000 *Science* **28** 604

[7] Song B S, Noda S and Asano T 2003 *Science* **300** 1537

[8] Noda S, Imada M, Ogawa S, Mochizuki M and Chutinan A 2002 *IEEE J. Quantum Electron.* **38** 726

[9] Lourtioz J M, Benisty H, Chelnokov A, David S and Olivier S 2003 *Ann. Telecommun.* **58** 2003 1197

[10] Yablonovitch E 1987 *Phys. Rev. Lett.* **58** 2059

[11] John S 1987 *Phys. Rev. Lett.* **58** 2486

[12] Dowling J P, Scalora M, Bloemer M J and Bowden C M 1994 *J. Appl. Phys.* **75** 1896

[13] Yablonovitch E, Gmitter T J, Meade R D, Rappe A M, Brommer K D and Joannopoulos J D 1991 *Phys. Rev. Lett.* **67** 3380

[14] Ozbay E and Temelkuran B 1996 *Appl. Phys. Lett.* **69** 743

[15] Yariv A, Xu Y, Lee R K and Scherer A 1999 *Opt. Lett.* **24** 711

[16] Ozbay E, Michel E, Tuttle G, Biswas R W, Ho K M, Bostak J and Bloom D M 1994 *Appl. Phys. Lett.* **65** 1617

[17] Temelkuran B, Ozbay E, Kavanaugh J P, Tuttle G and Ho K M 1998 *Appl. Phys. Lett.* **72** 2376

[18] Bayindir M and Ozbay E 2000 *Phys. Rev. B* **62** R2247

[19] Bayindir M, Tanriseven S and Ozbay E 2001 *Appl. Phys. A—Mater. Sci. Process.* **72** 117

[20] Ozbay E, Bayindir M, Bulu I and Cubukcu E 2002 *IEEE J. Quantum. Electron.* **83** 837

[21] Kosaka H, Kawashima T, Tomita A, Notomi M, Tamamura T, Sato T and Kawakami S 1998 *Phys. Rev. B* **58** R10096

[22] Notomi M 2000 *Phys. Rev. B* **62** 10696

[23] Gralak B, Enoch S and Tayeb G 2000 *J. Opt. Soc. Am.* A **17** 1012

[24] Luo C, Johnson S G, Joannopoulos J D and Pendry J B 2002 *Phys. Rev. B* **65** 201104

[25] Foteinopoulou S, Economou E N and Soukoulis C M 2003 *Phys. Rev. Lett.* **90** 107402

[26] Foteinopoulou S and Soukoulis C M 2003 *Phys. Rev. B* **67** 235107

[27] Parimi P V, Lu W T, Vodo v, Sokoloff J, Derov J S and Sridhar S 2004 *Phys. Rev. Lett.* **92** 127401

[28] Parimi P V, Lu T W, Vodo P and Sridhar S 2003 *Nature* **426** 404

[29] Cubukcu E, Aydin K, Ozbay E, Foteinopoulou S and Soukoulis C M 2003 *Nature* **423** 604
Cubukcu E, Aydin K, Ozbay E, Foteinopoulou S and Soukoulis C M 2003 *Phys. Rev. Lett.* **91** 207401

[30] Guven K, Aydin K, Alici K B, Soukoulis C M and Ozbay E 2004 *Phys. Rev. B* **70** 205125

[31] Pendry J B 2000 *Phys. Rev. Lett.* **85** 3966

[32] Luo C, Johnson S G, Joannopoulos J D and Pendry J B 2003 *Phys. Rev. B* **68** 045115

[33] Wang X, Ren Z F and Kempa K 2004 *Opt. Exp.* **12** 2919

[34] He S, Ruan Z, Chen L and Shen J 2004 *Phys. Rev. B* **71** 235115

[35] Moussa R, Foteinopoulou S, Zhang L, Tuttle G, Guven K, Ozbay E, and Soukoulis C M 2005 *Phys. Rev. B* **71** 085106

[36] Lu Z, Shi S, Schuetz C and Prather D 2005 *Opt. Express.* **13** 2007

[37] Wang X, Ren Z F and Kempa K 2005 *Appl. Phys. Lett.* **86** 061105

[38] Feng Z, Zhang X, Ren K, FEng S, Li Z-Y, Cheng B and Zhang D 2006 *Phys. Rev. B* **73** 075118

[39] Gonzalo R, de Maagt P and Sorolla M 1999 *IEEE Trans. Microw. Theory Tech.* **47** 2131

[40] Fehrembach A L, Enoch S and Sentenac A 2001 *Appl. Phys. Lett.* **79** 4280

[41] Qiu M and He S 2001 *Microw. Opt. Technol. Lett.* **30** 41

[42] Temelkuran B, Bayindir M, Ozbay E, Biswas R, Sigalas M M, Tuttle G and Ho K-M 2000 *J. Appl. Phys.* **87** 603

[43] Enoch S, Gralak B and Tayeb G 2002 *Appl. Phys. Lett.* **81** 1588

[44] Bulu I, Caglayan H and Ozbay E 2003 *Appl. Phys. Lett.* **83** 3263

[45] Koenderink A F and Vos W L 2003 *Phys. Rev. Lett.* **91** 213902

[46] Kosaka H, Kawashima T, Tomita A, Notomi M, Tamamura T, Sato T and Kawakami S 1999 *Appl. Phys. Lett.* **74** 1212

[47] Chigrin D N, Enoch S, Torres C M S and Tayeb G 2003 *Opt. Express.* **11** 1203

[48] Martinez A, Miguez H, Griol A and Marti J 2004 *Phys. Rev. B* **69** 165119

[49] Bulu I, Caglayan H and Ozbay E 2005 *Opt. Lett.* **30** 3078

[50] Ruan Z C, Qiu M, Xiao S S, He S L and Thylén L 2005 *Phys. Rev. B* **71** 045111